Plasma Phys. Control. Fusion **51** (2009) 085001 (12pp) doi:10.1088/0741-3335/51/8/085001

Observations of abrupt changes in the fluctuation spectrum on LMD-U

H Arakawa[1], K Kamataki[1], S Inagaki[2], T Maruta[1], Y Nagashima[3], T Yamada[3], S Shinohara[1], K Terasaka[1], S Sugita[1], M Yagi[2], N Kasuya[4], A Fujisawa[4], S-I Itoh[2] and K Itoh[4]

[1] Interdisciplinary Graduate School of Engineering Sciences, Kyushu University, 6-1 Kasuga-Koen, Kasuga 816-8580, Japan
[2] Research Institute for Applied Mechanics, Kyushu University, 6-1 Kasuga-Koen, Kasuga 816-8580, Japan
[3] Graduate School of Frontier Sciences, The University of Tokyo, 5-1-5 Kashiwanoha, Kashiwa 277-8561, Japan
[4] National Institute for Fusion Science, 322-6 Oroshi-cho, Toki 509-5292, Japan

E-mail: arakawa@riam.kyushu-u.ac.jp

Received 2 April 2009, in final form 25 May 2009
Published 30 June 2009
Online at stacks.iop.org/PPCF/51/085001

Abstract
A transition of the fluctuation spectrum of ion saturation current is observed in linear magnetized plasmas. A power spectrum with regular peaks and a broadband spectrum appear alternately during a discharge. The temporal order of changes in the modes is investigated at the transition. The low poloidal mode number components change before the higher modes begin to change. The delay times of change between modes are determined.

(Some figures in this article are in colour only in the electronic version)

1. Introduction

Turbulence-driven transport is one of the most important issues to be clarified in the realization of a thermonuclear fusion reactor. Electrostatic turbulence, especially drift wave turbulence, has thus been extensively investigated. It is known that the fluctuations of various spatial and temporal scales exist in turbulent plasmas [1, 2], and their mutual interactions can generate meso-scale structures, such as zonal flows and streamers [3, 4]. (See reviews of experiments, e.g. [5, 6].) The turbulence and structure co-exist and plasmas are governed by competing processes of different time scales. The time scale of turbulence–structure formation, therefore, is crucial to clarify the competing and/or cooperative mechanisms between fluctuations. Turbulent plasmas often show fast time scale phenomena (e.g. L–H transitions [7–11] and transit transport [12–15]). However, temporal sequences in the evolution of fluctuations and its time scales at the transition have not been reported in a systematic manner. Studies on devices for basic experiments have shown considerable progress [16, 17], but more precise

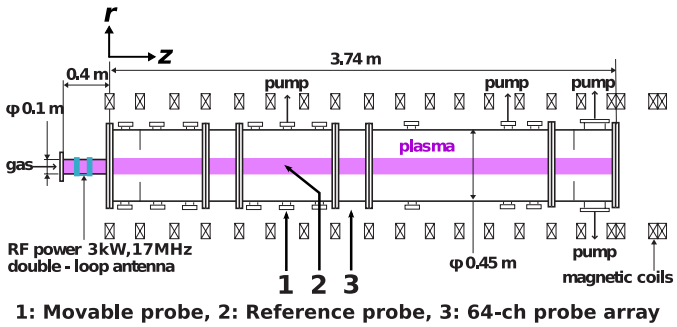

Figure 1. Schematic view of the LMD-U and diagnostic tools (1: movable probe, 2: reference probe ($r = 4$ cm), 3: 64-ch probe array ($r = 4$ cm)).

observations are needed. For a more comprehensive understanding of turbulent transport mechanisms, it is primarily important to observe transition phenomena of turbulence and to identify the time scale of the turbulence–structure formation. In particular, measurement of the energy transfer time in the wave-number space gives a basic insight into structure formation in the turbulent plasma. It would be worth comparing the delay time for the higher harmonics with theoretical discussions at the transition.

In this paper, an abrupt change in the density fluctuation in a linear magnetized plasma is studied. A wave-number spectrum is decomposed and temporal evolutions of each poloidal-Fourier component are analyzed. The time scale of change in fluctuation at the onset of the transition is measured. Delays in the response of higher harmonics compared with that of primary components are quantified.

2. Experimental setup

The turbulence excitation experiments were performed on the Large Mirror Device Upgrade (LMD-U) [4, 18]. A schematic view of the LMD-U and diagnostic tools is shown in figure 1. A cylindrical plasma with a diameter of approximately 0.1 m and an axial length of 3.74 m is produced by the RF wave in a quartz tube (axial length = 0.4 m and inner diameter 0.095 m) and radially confined by the magnetic field (z: axial, r: radial, θ: poloidal direction). The typical operational condition and plasma parameters are 3 kW RF power, 0.09 T magnetic field, 1–5 mTorr neutral gas pressure (argon), 6×10^{18} m^{-3} peak electron density and 3 eV electron temperature. The diagnostic tools are a 64-channel poloidal Langmuir probe array [19], a movable Langmuir probe [4] and a reference probe. The axial and radial positions of the 64-channel probe array in LMD-U are $z = 1.885$ m and $r = 4$ cm (probe tips are 0.39 cm apart). A movable probe, which is movable in the radial direction, is installed at the axial position of 1.375 m. The reference probe is installed at $z = 1.375$ m and $r = 4$ cm.

3. Spectrum transition during a discharge

In LMD-U plasmas, the time evolution and power spectrum of the ion saturation current, I_{is}, vary depending on the neutral gas pressure, P_n, as shown in figure 2 [20, 21]. Figures 2(a) and (b) show the power spectrum of $\tilde{I}_{is}$ by the 64-ch poloidal probe array which decomposed the θ–t space into the m–f space, where t is the time, m is the poloidal mode number and f is the frequency of fluctuations [22]. Here the time window of the power spectrum is 4096 μs

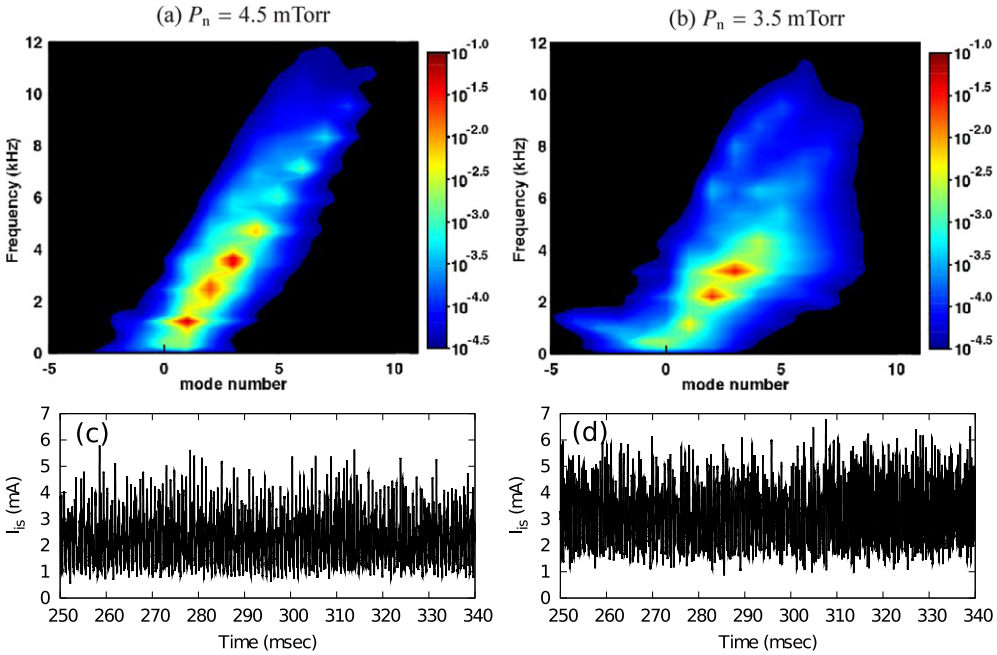

Figure 2. Power spectrum of $\tilde{I}_{is}$ in the high neutral pressure case (a) and the low pressure case (b) by the 64-ch poloidal probe array. (The time window of the spectrum is 4096 μs and the 121 ensembles are averaged.) Typical time evolution of I_{is} for each case (c) and (d).

and the 121 ensembles are averaged. In the high neutral pressure case (figure 2(a)), the power spectrum has some peaks, which lie along a straight line in the $m-f$ space. The higher-m modes are considered to be produced by nonlinear wave coupling effects (e.g. frequency doubling) [23, 24]. Actually, nonlinear wave coupling between modes was identified in LMD-U [4, 25, 26]. In the low neutral pressure case (figure 2(b)), broadband components are developed. One must notice that the $m = -1$ component, which plays an important role in the streamer formation [4], appears in the low pressure case. In both cases, the turbulence is saturated and becomes stationary as shown in figures 2(c) and (d). The apparent phase velocities of the main fluctuation peaks are estimated to be 3.0×10^2 m s^{-1} and 2.7×10^2 m s^{-1} for the high and low neutral pressure cases, respectively.

In the marginal neutral pressure condition (3.5–4.3 mTorr), the power spectrum changes abruptly during a discharge [20, 21, 27]. The jumps occur repeatedly. A typical time evolution of I_{is} at 4 mTorr is shown in figure 3(a). The I_{is} has two states (lower and higher fluctuation levels) and the discharge alternatively moves between those states. In addition, the reflected RF power also changes simultaneously (figure 3(b)). Such abrupt changes (over 20%) in the reflected power are not observed in the higher/lower neutral pressure cases. We define here the state of turbulence with higher/lower reflected power to be state A/B. The power spectra of states A and B are shown in figure 3(c) and (d), respectively. The time window of the spectrum is 4096 μs and the 298 ensembles are averaged in both the cases. The power spectra, which are similar to the regular-peak spectrum in state A and the one similar to the broader spectrum in state B, are observed, respectively. The apparent phase velocities of the main peaks in states A and B are close to that for the $P_n = 4.5$ mTorr and 3.5 mTorr cases, respectively. These abrupt changes in turbulence are therefore considered to be transitions between the turbulence with a regular-peak spectrum and the one with a broader spectrum.

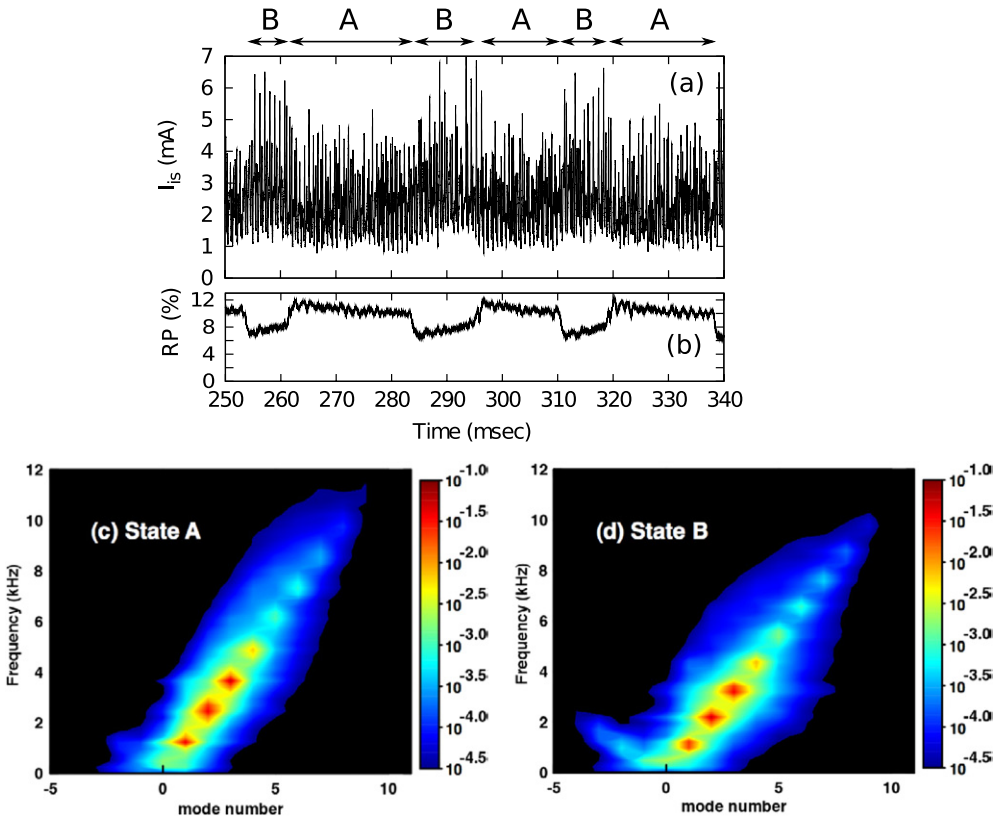

Figure 3. Typical time evolution of (*a*) I_{is} and (*b*) reflected RF power (RP) at 4 mTorr. The power spectrum in state A (*c*) and state B (*d*). (The time window of the spectrum is 4096 μs and the 298 ensembles are averaged.)

Figure 4 shows the typical radial profiles of the time averaged I_{is}, $\bar{I_{is}}$, inverse scale-length, $\nabla\bar{I_{is}}/\bar{I_{is}}$, floating potential, $\bar{V_f}$ and gradient of floating potential, $\nabla\bar{V_f}$ in both the A and B states. They are measured using the movable probe and the average is defined as

$$\bar{I_{is}}(r) = \frac{1}{N}\sum_{i=1}^{N}\left\{\frac{1}{W}\sum_{q=0}^{W-1}\left(I_{is}(r,t_q)\right)_i\right\}, \tag{1}$$

$$\frac{\nabla\bar{I_{is}}}{\bar{I_{is}}}(r) = \frac{\bar{I_{is}}(r+\Delta r/2)-\bar{I_{is}}(r-\Delta r/2)}{\Delta r}\cdot\frac{1}{\bar{I_{is}}(r)}, \tag{2}$$

$$\bar{V_f}(r) = \frac{1}{N}\sum_{i=1}^{N}\left\{\frac{1}{W}\sum_{q=0}^{W-1}\left(V_f(r,t_q)\right)_i\right\}, \tag{3}$$

$$\nabla\bar{V_f}(r) = \frac{\bar{V_f}(r+\Delta r/2)-\bar{V_f}(r-\Delta r/2)}{\Delta r}. \tag{4}$$

Here, the ensemble of the observed A or B state is given by N. In each observation of a period A (or B), we perform the time average over the time window $W\Delta t$, using measured values at

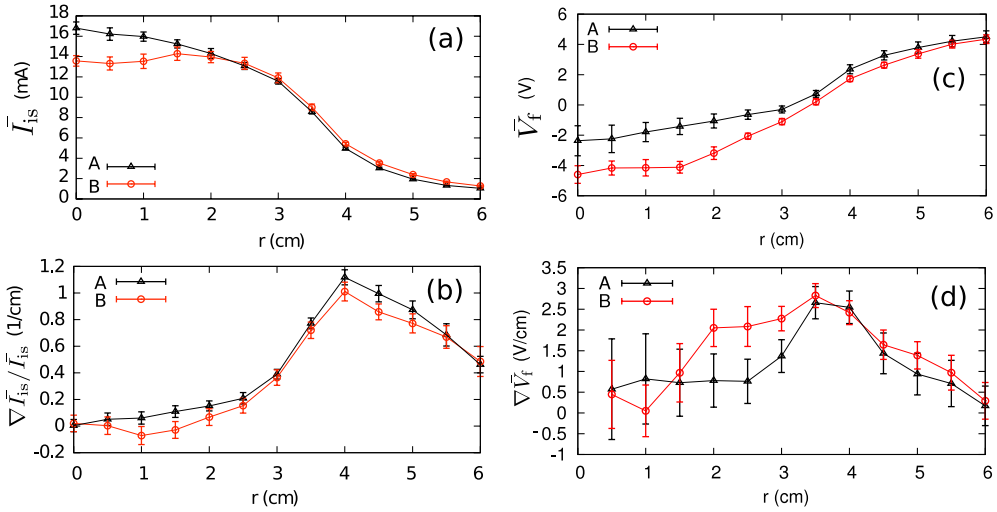

Figure 4. Radial profile of (*a*) ion saturation current, (*b*) inverse scale-length, (*c*) floating potential and (*d*) gradient of floating potential.

$t_q = t_0 + q\Delta t$. (The time window between t_0 and $t_0 + W\Delta t$ is defined for each realization of state A or B.) We use $N = 21$ ensembles, $W = 2048$, $\Delta t = 1\,\mu$s, $\Delta r = 1$ cm and integer of i and q in this case. The measurement positions are 0–6 cm with 0.5 cm intervals. The small effect of probe insertion is monitored with a reference probe measuring the ion saturation current located at fixed-position ($r = 4$ cm) and compensated for. Standard deviations of N ensembles are shown by error-bars for $\bar{I}_{\rm is}$ and $\bar{V}_{\rm f}$. The $\sigma_{\nabla \bar{I}_{\rm is}/\bar{I}_{\rm is}}$ (errors of $\nabla \bar{I}_{\rm is}/\bar{I}_{\rm is}$) and $\sigma_{\nabla \bar{V}_{\rm f}}$ (error of $\nabla \bar{V}_{\rm f}$) are defined here as

$$\sigma_{\nabla \bar{I}_{\rm is}/\bar{I}_{\rm is}}(r) = \frac{1}{\bar{I}_{\rm is}(r)} \sqrt{\frac{1}{(\Delta r)^2}\left\{\sigma^2_{\bar{I}_{\rm is}}(r + \Delta r/2) + \sigma^2_{\bar{I}_{\rm is}}(r - \Delta r/2)\right\} + \left(\frac{\nabla \bar{I}_{\rm is}(r)}{\bar{I}_{\rm is}(r)}\right)^2 \sigma^2_{\bar{I}_{\rm is}}(r)}, \tag{5}$$

$$\sigma_{\nabla \bar{V}_{\rm f}}(r) = \frac{1}{2\Delta} \sqrt{\sigma^2_{\bar{V}_{\rm f}}(r + \Delta r/2) + \sigma^2_{\bar{V}_{\rm f}}(r - \Delta r/2)}, \tag{6}$$

where $\sigma_{\bar{I}_{\rm is}}$ and $\sigma_{\bar{V}_{\rm f}}$ are errors (standard deviation) of $\bar{I}_{\rm is}$ and $\bar{V}_{\rm f}$, respectively.

$\bar{I}_{\rm is}$ in state A has a center-peaked profile and a hollow one in state B. $\bar{I}_{\rm is}$ in the region of $r = 2.5$–6 cm is slightly larger in state B than that in state A. The inverse scale-length, $\nabla \bar{I}_{\rm is}/\bar{I}_{\rm is}$, has a maximum at $r = 4$ cm in both cases. $\nabla \bar{I}_{\rm is}/\bar{I}_{\rm is}$ shows that it is greater in state A but the difference is not clear because of insufficient statistics. The relative change in $\bar{V}_{\rm f}$ is larger than the one in $\bar{I}_{\rm is}$. $\bar{V}_{\rm f}$ profile in state A is larger than that in state B. The time delay of the change in the $I_{\rm is}$ profile from the transition is discussed later.

4. Time evolution of the poloidal Fourier components at transitions

To understand the abrupt change in the turbulent state, we analyze the time evolution of fluctuations at the onset of turbulence transitions by using the instantaneous mode amplitude technique. Fourier transform in the poloidal wave number is applied to the instantaneous signals of a 64-ch poloidal probe array $I(\theta, t)$, where $\theta = 2\pi i/M$, $M = 64$ and i is an integer.

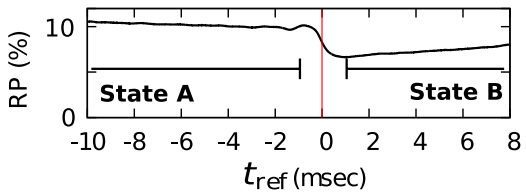

Figure 5. The time evolution of the ensemble averaged (674 in this case) reflected power and the definition of the time of transition. We define here the time of transition ($t_{ref} = 0$) at the inflection point of reflected power as indicated by the vertical red line.

Then, the poloidal wave-number-decomposed fluctuation,

$$\hat{I}(m,t) = \frac{1}{M}\sum_{i=0}^{M-1} I(2\pi i/M, t)\exp\left[2\pi \mathrm{j}\left(-\frac{im}{M}\right)\right], \tag{7}$$

is obtained; here m is the poloidal mode number and j is the imaginary unit ($\mathrm{j}^2 = -1$). In order to study the dynamics at the transition, we define here the time of transition ($t_{ref} = 0$) at the inflection point of reflected power (figure 5). Figure 6 shows the time evolution of the ensemble averaged power spectrum,

$$\langle P(m,t)\rangle = \frac{1}{N}\sum_{i=1}^{N} |\hat{I}_i(m,t)|^2, \tag{8}$$

of the modes with low-m, high-m and middle-m mode numbers over the transition from state A to B, here $N = 674$ ensembles are averaged. In the ensemble averaging, every time window is synchronized with respect to the transitions by using the cross-correlation technique. The timing of transitions is detected from the inflection point of the reflected power and each time window is chosen so that the cross-correlation between the reflected power in target time window and the one in the reference window yields the maximum. The cross-correlation function (CCF) is defined as

$$C_{xy}(\tau\Delta t) = \begin{cases} \dfrac{\dfrac{1}{W-\tau}\displaystyle\sum_{i=\tau}^{W-1}(x(t_i)-\bar{x})(y(t_i-\tau\Delta t)-\bar{y})}{\sqrt{\dfrac{1}{W}\displaystyle\sum_{i=0}^{W-1}(x(t_i)-\bar{x})^2}\sqrt{\dfrac{1}{W}\displaystyle\sum_{i=0}^{W-1}(y(t_i)-\bar{y})^2}}, & \tau\Delta t \geqslant 0, \\ C_{yx}(-\tau\Delta t), & \tau\Delta t < 0, \end{cases} \tag{9}$$

where Δt is 1 μs, $\tau\Delta t$ is the delay time, $W\Delta t$ is the time window which covers around the transition (we choose 20 ms), $x(t_i)$ and $y(t_i)$ are the time series data (of reflected power) and $\bar{x}$ and $\bar{y}$ are the ensemble average of $x(t_i)$ and $y(t_i)$.

The time evolutions of each mode are quite different between $m = 0$–3 (low-m) modes and $m \geqslant 8$ (high-m) modes. Amplitudes of low-m modes change before reduction in the reflected power ($t_{ref} < 0$ ms). On the other hand, high-m modes change after reduction in the reflected power ($t_{ref} > 0$ ms). The lower-m modes ($m = 1$–3) are considered to satisfy the wave-dispersion relations [26, 28] and the higher-m modes ($m \geqslant 4$) are considered to be driven by the nonlinear coupling between the lower-m modes [4, 25]. The amplitudes of the $m = 4$–7 (middle-m) modes exhibit the intermediate time evolution between those of the

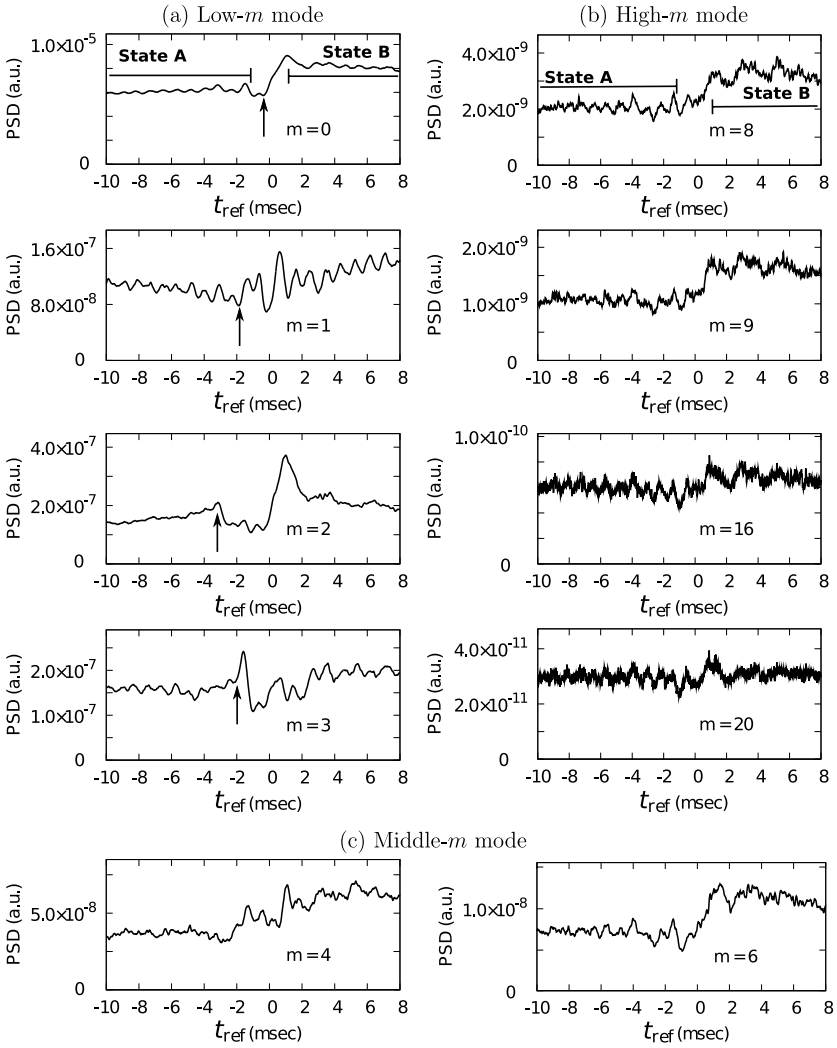

Figure 6. The time evolution of the mode amplitude at different poloidal mode numbers: (*a*) low-*m* modes, (*b*) high-*m* modes and (*c*) middle-*m* modes. The 674 ensembles are averaged.

low-*m* and high-*m* modes as shown in figure 6(*c*). The middle-*m* modes respond abruptly just as the lower-*m* modes. And like the higher-*m* modes, the amplitude of the middle-*m* modes is increased after the transition. The temporal sequence of transition is discussed in detail with respect to three different mode number regions.

The $m = 0$ mode changes abruptly at -0.5 ms. Changes in the other low-*m* modes (1, 2 and 3) are also triggered from -3.5 to -1.5 ms. With respect to the $m = 1$ mode, the power starts to fluctuate after -2 ms. This fluctuation may be due to the fact that state B includes $m = 1$ and $m = -1$ modes and the instantaneous mode amplitude technique cannot distinguish them. Other negative *m* modes are negligible because the power of the positive *m* modes is 10 or more times larger than that of the negative ones.

In order to establish the unambiguous observation of the temporal sequence of the changes in the lower-*m* modes, the statistical convergence analysis is performed with respect to peaks

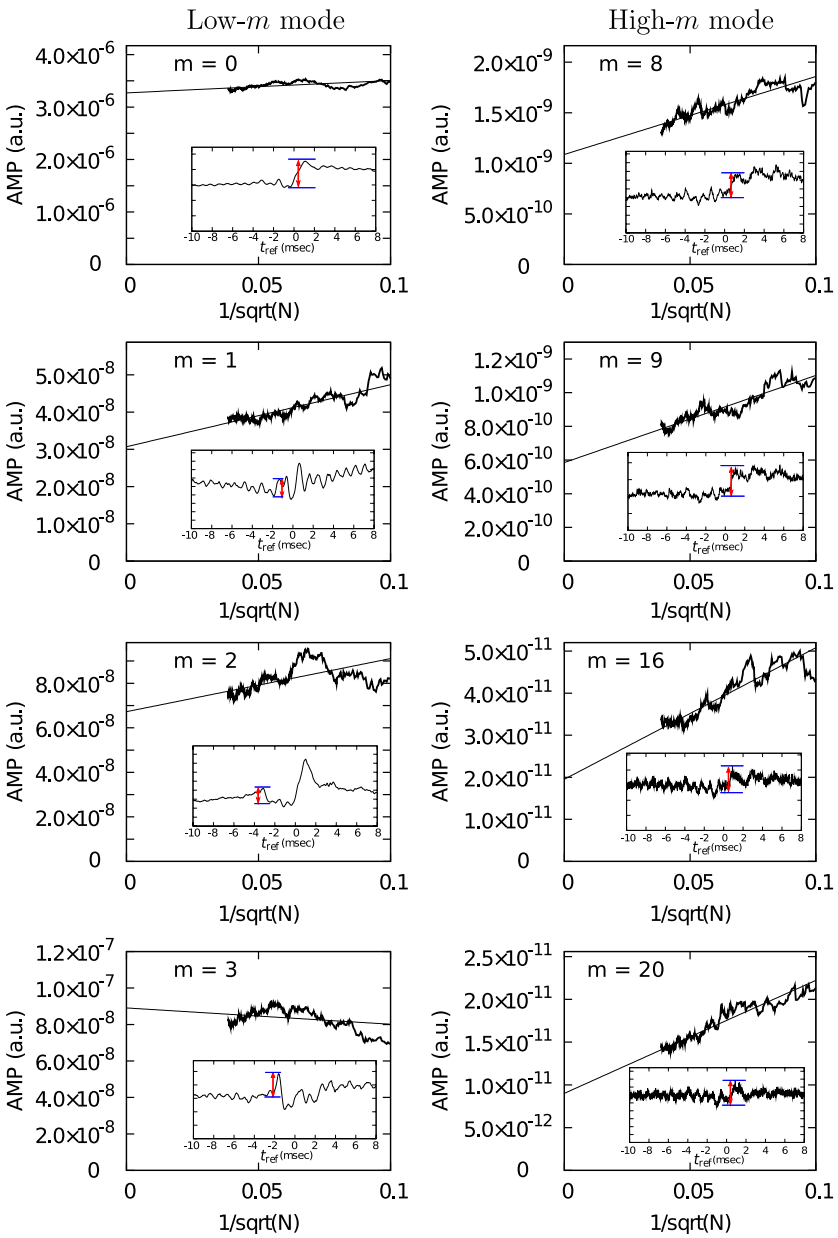

Figure 7. Convergence analysis of the amplitude of the changes observed in figure 6.

and gaps observed in the time evolution of the modes. Figure 7 shows the variation in the amplitude of each mode as a function of the number of ensemble N (i.e. the number of observed transitions). The variations are defined as peak-to-peak values during -0.5 to 2 ms (for $m = 0$, 8, 16 and 20 modes), -2 to -1 ms (for $m = 1$ mode), -4 to -2.5 ms (for $m = 2$ mode) and -3 to -1.5 ms (for $m = 3$ mode), respectively and are shown in sub-figures. In the limit of $N \to \infty$, the variations converge to the finite values for $m \leqslant 20$ modes. Thus the temporal change in $\langle P(m,t)\rangle$ discussed here is not a random

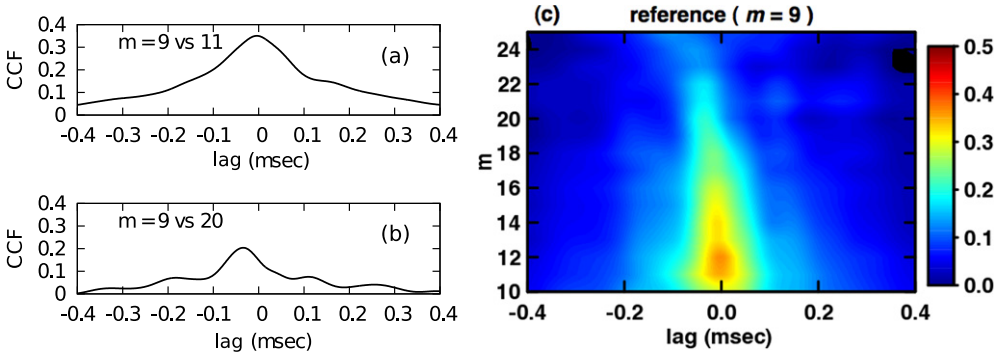

Figure 8. Cross-correlation functions between (*a*) $m = 9$ and 11 modes and (*b*) $m = 9$ and 20 modes. (*c*) Contour map of the cross-correlation function between $m = 9$ and $m = 11$–25 modes. Each time window is 20 ms and the 674 ensembles are averaged.

variation but an unambiguous dynamical change at the onset of A → B states transition. One can conclude that the averaging by use of 674 observations provides a significant data set for the analysis.

From the results of the convergence analysis, the temporal sequence of the transition is determined and the onset of transitions for each mode is shown in figure 6 by arrows. The $m = 2$ mode begins to change first of all. The sequence of change between $m = 1$ and 3 modes cannot be distinguished since these changes take place simultaneously within 0.2 ms. This may be because the $m = 1$ and 3 modes are coupled strongly through non-linear processes involving the $m = 2$ mode. The order of the change in the modes shows that the transition sequence is $m = 2 \rightarrow$ (1 and 3) $\rightarrow 0$. The change in the background profile reflects one in the $m = 0$ mode, thus it is considered to be a result of the transition.

The temporal sequence of change between the higher-m modes is unclear in figure 6. We analyze the delays at the onset of the transition of the high-m modes by using the cross-correlation technique. Figures 8(*a*) and (*b*) show the ensemble averaged (674 in this case) cross-correlation function between the amplitudes of the $m = 9$ and 11 modes and those of $m = 9$ and 20 modes over the transition. Here, the time window is 20 ms, the negative time lag of the cross-correlation function means that the change in the $m = 9$ mode has a delay compared with the reference one and the uncertainty is determined from the standard deviation of the cross-correlation function. The peaks of the cross-correlation function indicate that the $m = 9$ mode has a 0.00 ± 0.09 ms delay compared with the $m = 11$ mode and has a 0.03 ± 0.06 ms delay compared with the $m = 20$ mode. The cross-correlation function between the $m = 11$–25 modes and a reference one ($m = 9$) is calculated and shown in figure 8(*c*). The change in high-m modes cannot be discriminated within the uncertainty, and thus those occur simultaneously within ± 0.1 ms. However, there may be a trend to change from the higher-m modes to the lower-m modes as shown in figure 8(*c*).

The temporal sequence of the middle-m modes ($m = 4$–7) is unclear. This is because the middle-m modes are strongly coupled through various combinations of the change in low-m modes. The cross-correlation function between the $m = 4$ and 7 modes is shown in figure 9. The peaks denote that the $m = 7$ mode has a 0.0 ± 0.3 ms delay in comparison with the $m = 4$ mode. Compared with the cross-correlation functions between the high-m modes, the uncertainty determined from the standard deviation becomes large. All cross-correlation functions between the middle-m modes are broader. Based on this analysis, the transitions of the middle-m modes occur simultaneously within ± 0.3 ms.

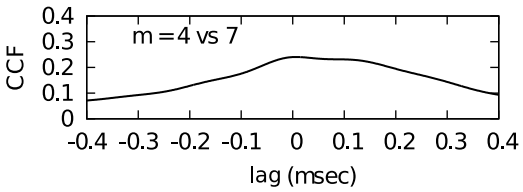

Figure 9. The ensemble averaged cross-correlation function between $m = 4$ and 7 mode.

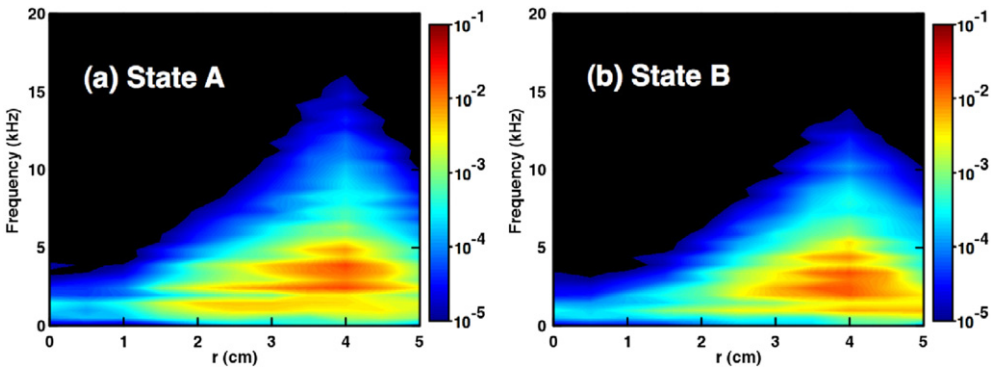

Figure 10. The radial amplitude of fluctuations on each mode in states A (*a*) and B (*b*). The time window of the spectrum is 2048 μs and the 21 ensembles are averaged.

The spatial structure of fluctuation also affects the time sequence of the event during the transition. Figure 10 shows the radial amplitude of fluctuations, $Z(r, f)$, for each mode obtained from the Fourier transform of $\tilde{I}_{\rm is}/\bar{I}_{\rm is}$:

$$Z(r, f) = \frac{1}{W}\sum_{i=0}^{W-1}\left(\tilde{I}_{\rm is}(r, t)/\bar{I}_{\rm is}(r)\right)\exp\left[2\pi {\rm j}\left(-\frac{iq}{W}\right)\right], \tag{10}$$

where $f = q/(W\Delta t)$, Δt is the sampling time (1 μs in this case), $W\Delta t$ is the time window (we choose 2048 μs), N is the number of ensemble (21 in this case), i and q are integers and j is the imaginary unit. Every radial amplitude of fluctuations has a peak at $r = 4$ cm where the 64-ch probe array is located and the instantaneous amplitude technique is applied. Thus, the temporal order during the transition events in fluctuations at $r = 4$ cm reflects that of the overall transition feature of the plasma. In addition, from the signals of a poloidal probe array and of a probe set aligned in the same magnetic field line, we may say that the transition takes place simultaneously both in the poloidal and in the parallel directions.

5. Summary and discussion

In summary, we investigated the transition phenomena of the ion saturation current in a low temperature linear plasma. The experimental observations show the following

(i) Two steady turbulence states are realized in the different neutral pressure regimes in LMD-U.
(ii) Repetition of forward and backward transitions between two turbulence states are observed at the critical neutral pressure.

(iii) Time evolutions of poloidal mode-number-expanded fluctuations are obtained by using the instantaneous mode amplitude technique.

(iv) In the lower-m modes, the transition takes place in the order of $m = 2 \rightarrow (1 \text{ and } 3) \rightarrow 0$. The $m = 1$–3 modes change before the change in the reflected power.

(v) In the higher-m modes, modes change simultaneously within an accuracy of 0.1 ms.

(vi) In the middle-m modes, modes change simultaneously within an accuracy of 0.3 ms.

Fourier components with high mode numbers are driven by unstable lower-m modes through the nonlinear processes. The transfer time in the k-space, τ_t, by which high-m modes obtain the energy via Lagrange nonlinearity in dynamical equation, has been estimated as $\tau_t^{-1} \sim \tilde{V}k$, the eddy-scrambling rate ($\tilde{V}$: the $E \times B$ fluctuation velocity, k: the typical wave number) [29]. For the experimental conditions, $\tilde{V} \sim 500\,\mathrm{m\,s^{-1}}$ (by the estimation of the fluctuation electric field of $50\,\mathrm{V\,m^{-1}}$ and magnetic field of $B \sim 0.09\,\mathrm{T}$) and $k \sim 50\,\mathrm{m^{-1}}$ for $m = 2$, one obtains the evaluation of $\tau_t \sim 40\,\mu\mathrm{s}$. The observation, i.e. the high-m modes change simultaneously within an accuracy of $100\,\mu\mathrm{s}$, is consistent with the expectation that the transfer in the k-space takes place within the time scale of τ_t. In addition, the degrees of freedom of the excited components are of the order of 10. In the case of such a small number of degrees of freedom, the energy transfer may not be a monotonic flow into larger-m modes (à la Kolmogorov cascade), but may be bound in the Fourier space as has been discussed in [29]. The large width of the cross-correlation function (shown in figure 9) supports the view that such a complicated transfer of energy takes place in the Fourier space.

Acknowledgments

This work is partly supported by a grant-in-aid for Specially Promoted Research of MEXT of Japan (16002005), the grant-in-aid for Scientific Research C (20560767) and by the collaboration programmes of RIAM of Kyushu University and of NIFS (NIFS07KOAP017).

References

[1] Itoh S-I and Itoh K 2001 *Plasma Phys. Control. Fusion* **43** 1055–102
[2] Diamond P H, Itoh S-I, Itoh K and Hahm T S 2005 *Plasma Phys. Control. Fusion* **47** 35–161
[3] Fujisawa A *et al* 2004 *Phys. Rev. Lett.* **93** 165002
[4] Yamada T *et al* 2008 *Nature Phys.* **4** 721
[5] Fujisawa A *et al* 2007 *Nucl. Fusion* **47** 718
[6] Fujisawa A 2009 *Nucl. Fusion* **49** 013001
[7] Wagner F *et al* 1982 *Phys. Rev. Lett.* **49** 1408–12
[8] Wagner F *et al* 1984 *Phys. Rev. Lett.* **53** 1453–6
[9] Itoh S-I and Itoh K 1988 *Phys. Rev. Lett.* **60** 2276–9
[10] Fujisawa A *et al* 1997 *Phys. Rev. Lett.* **79** 1054–7
[11] Ido T, Kamiya K, Miura Y, Hamada Y, Nishizawa A and Kawasumi Y 2002 *Phys. Rev. Lett.* **88** 55006
[12] Wagner F and Stroth U 1992 *Plasma Phys. Control. Fusion* **34** 1803
[13] Gentle K W *et al* 1995 *Phys. Rev. Lett.* **74** 3620–3
[14] Stroth U, Itoh K, Itoh S-I, Hartfuss H and Laqua H 2001 *Phys. Rev. Lett.* **86** 5910–3
[15] Inagaki S *et al* 2008 *J. Plasma Fusion Res.* **3** S1006
[16] Tynan G R, Holland C, Yu J H, James A, Nishijima D, Shimada M and Taheri N 2006 *Plasma Phys. Control. Fusion* **48** 51
[17] Sokolov V, Wei X, Sen A K and Avinash K 2006 *Plasma Phys. Control. Fusion* **48** 111
[18] Shinohara S *et al* and Institute of Plasma Physics, AS CR, Prague, 2007 *Proc. 28th Int. Conf. on Phenomena in Ionized Gases (Prague, Czech Republic)* 1P04-08 pp 354–7
[19] Yamada T *et al* 2007 *Rev. Sci. Instrum.* **78** 123501

[20] Nagashima Y *et al* 2006 Drift wave turbulence in helicon high-density linear plasma II: fluctuation dynamics *48th Annual Meeting of the Division of Plasma Physics (30 October–3 November 2006)* (American Physical Society) abstract# JP1. 087
[21] Nagashima Y *et al* 2007 Identification of the parametric-modulational instability of the drift wave-zonal flow system in a cylindrical magnetized plasma *49th Annual Meeting of the Division of Plasma Physics (12–16 November 2007)* (American Physical Society) abstract# YP8. 073
[22] Yamada T *et al* 2008 *Plasma Fusion Res.* **3** 044
[23] Itoh S-I, Itoh K and Mori H 2006 *J. Phys. Soc. Japan* **75** 034501
[24] Yagi M, Ueda T, Itoh S-I, Azumi M, Itoh K, Diamond P H and Hahm T S 2006 *Plasma Phys. Control. Fusion* **48** A409–A418
[25] Yamada T *et al* 2007 *Plasma Fusion Res.* **2** 51
[26] Kasuya N, Yagi M, Itoh K and Itoh S-I 2008 *Phys. Plasmas* **15** 052302
[27] Nagashima Y *et al* 2008 *Int. Congress on Plasma Physics (ICPP) (Fukuoka, Japan)* FB.O1-X-3 p 387
[28] Kasuya N, Yagi M, Azumi M, Itoh K and Itoh S-I 2007 *J. Phys. Soc. Japan* **76** 044501
[29] Yoshizawa A, Itoh S-I and Itoh K 2002 *Plasma and Fluid Turbulence: Theory and Modelling* (Bristol: Institute of Physics Publishing)